Sensors & Actuators: B. Chemical 443 (2025) 138268

Contents lists available at ScienceDirect

Sensors and Actuators: B. Chemical

journal homepage: www.elsevier.com/locate/snb

Differentiated imaging of Hashimoto's thyroiditis against thyroid carcinoma by endogenous peroxynitrite activated near-infrared fluorescent probe

Wanwei Zhang [a], Mo Ma [a,b], Chen Zhao [a], Wenping Dong [a], Pinyi Ma [a], Daqian Song [a], Ying Sun [a,*]

[a] College of Chemistry, Jilin Province Research Center for Engineering and Technology of Spectral Analytical Instruments, Jilin University, Qianjin Street 2699, Changchun 130012, China
[b] School of Pharmacy, Jilin University, Qianjin Street 2699, Changchun 130012, China

ARTICLE INFO

Keywords:
Fluorescent probe, Near-infrared, Peroxynitrite
Hashimoto's thyroiditis

ABSTRACT

Hashimoto's thyroiditis is one of the most common autoimmune diseases. Due to the similarity of the traits, traditional examination methods may misdiagnose it as thyroid cancer in some cases. Accurate diagnosis of Hashimoto's thyroiditis can avoid organ resection by misdiagnosis of thyroid cancer, preserve organ function for patients and reduce surgical trauma. Here, we designed and synthesized a near-infrared fluorescent probe named HNTC-HT for differentiated imaging of Hashimoto's thyroiditis against thyroid carcinoma. Reactive oxygen species (ROS), such as peroxynitrite ($ONOO^-$), highly accumulated in Hashimoto's thyroiditis. While the content of ROS in thyroid cancer cells was significantly lower than that in Hashimoto's thyroiditis cells. $ONOO^-$ removes the trifluoromethanesulfonic acid group by affinity substitution reaction. And then HNTC-HT restores to fluorophore HNTC-OH which produces near-infrared fluorescence due to intramolecular charge transfer (ICT). We successfully perform differentiated imaging of Hashimoto's thyroiditis against thyroid carcinoma with HNTC-HT by the specific detection of intracellular $ONOO^-$. The fluorescence brightness of thyroiditis cells is much higher than thyroid cancer cells, which proves that the probe HNTC-HT can be used to effectively differentiate Hashimoto's thyroiditis against thyroid cancer cells. Satisfactory results were also obtained in subsequent mouse experiments. In this work, the fluorescence probe HNTC-HT activated by ROS has been more appropriately applied, so as to address the limit in the misdiagnosis of Hashimoto's thyroiditis as thyroid cancer, thus expanding potential applications of near-infrared fluorescent probe in the diagnosis of thyroid disease.

1. Introduction

Hashimoto's thyroiditis, characterized by serious decrease of thyroid function, is one of the most common clinical diseases in the world [1]. However, its insidious onset and slow progression always keep most patients asymptomatic in the early stage [2,3]. As the disease progresses, the patient's condition worsens if effective measures are not taken in time [4,5]. The histopathological features of Hashimoto's thyroiditis include lymphoblastic infiltration, follicular formation in the germinal center, and parenchymal atrophy [6–8]. Thyroid lymphocyte infiltration is the pathological feature of Hashimoto's thyroiditis, and it is also commonly appeared in thyroid carcinoma [9]. The current diagnostic methods for Hashimoto's thyroiditis include blood collection, ultrasound, biopsy and so on [10,11]. However, in some cases, these traditional methods cannot completely diagnose Hashimoto's thyroiditis, and may misdiagnose it as thyroid carcinoma [12,13]. Accurate diagnosis of Hashimoto's thyroiditis helps patients avoid thyroidectomy, thereby preserving thyroid function, avoiding surgical trauma and improving life quality of patients [3,14]. Previous studies have shown that oxidative stress caused by overexpression of ROS is closely related to various pathological changes of Hashimoto's thyroiditis [15]. Experimental studies in nonobese diabetic NOD.H2h4 mice suggest that thyroid accumulation of reactive oxygen species (ROS) contributes to the initiation and progression of Hashimoto's thyroiditis. These mice spontaneously develop thyroid peroxidase antibodies (TPOAb) and thyroglobulin antibodies (TgAb)[16]. Ruggieri et al. analyzed several

* Corresponding author.
E-mail address: yingsun@jlu.edu.cn (Y. Sun).

https://doi.org/10.1016/j.snb.2025.138268
Received 8 April 2025; Received in revised form 17 June 2025; Accepted 5 July 2025
Available online 7 July 2025

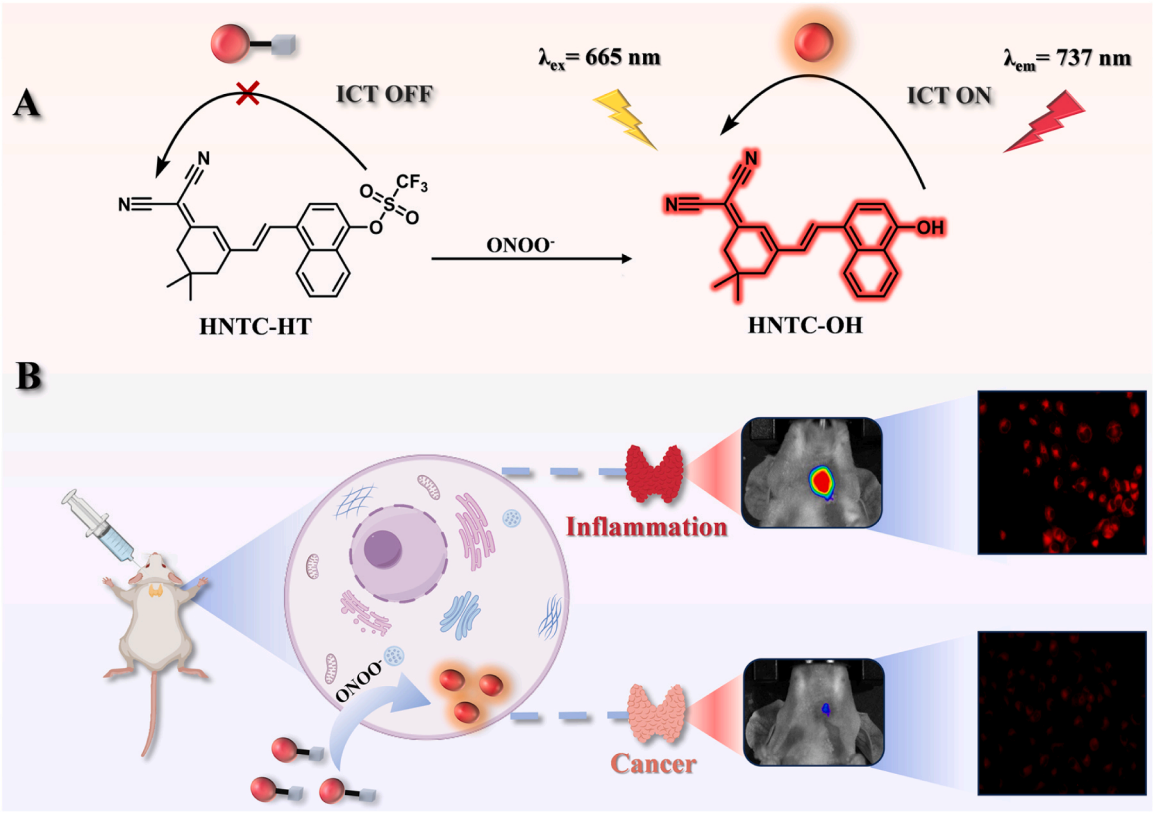

Scheme 1. (A) Reaction mechanism of HNTC-HT. (B) Illustration of near-infrared fluorescence imaging of $ONOO^-$ by HNTC-HT in Hashimoto's thyroiditis and thyroid carcinoma.

oxidative stress markers of patients suffered from Hashimoto's disease and healthy people, and found the thyroid ROS was highly expressed in the patients of Hashimoto's disease versus healthy controls [17]. On the other hand, cancer cells metabolize through glycolysis under hypoxia [18,19]. As for thyroid cancer, over-accumulated ROS can clear themselves [20,21], and the expression of ROS in thyroid cancer is significantly lower than that in inflammatory cells.

Peroxynitrite ($ONOO^-$), as one of the most important ROS, is produced by the combination of nitric oxide and superoxide anion radical [22]. $ONOO^-$ demonstrates superior stability and oxidative capacity compared to other ROS, making it an optimal target analyte for assessing oxidative stress levels [23,24]. Therefore, precise imaging of $ONOO^-$ can be used to differentiate Hashimoto's thyroiditis against thyroid carcinoma. So far, a variety of methods for detecting $ONOO^-$ have been reported, such as electrochemical and microbial methods [25,26]. However, most of these methods may cause cell or tissue damaged and prevent their further application. By contrast, fluorescent probes have many advantages such as biocompatibility, non-invasive, high sensitivity and visualization to monitor many physiological or pathological processes in real time [27–29]. Near-infrared fluorophore (emission region 650–1000 nm) shows a promising performance in biological applications [30,31]. It can not only penetrate deeper tissues, but also avoid the interference from bio autofluorescence [32,33]. While previous near-infrared fluorescence probes for the detection of $ONOO^-$ have some general limits, such as small stokes displacement, low fluorescence intensity, short emission wavelength, and weak penetrating ability of tissue, resulting in poor imaging results [34,35].

The bicyano-isoflurone near-infrared fluorescence probe has the advantages such as near-infrared emission and large Stokes shift [36]. In this paper, a ONOO− activated near-infrared fluorescence probe based on dicyano-isoflurone is designed and synthesized which named HNTC-HT. HNTC-HT has specific responding to ONOO−, rapid imaging with near-infrared fluorescence emission characteristics in cell and vivo. The sensing mechanism of HNTC-HT was studied by high performance liquid chromatography (HPLC) and liquid chromatography-high resolution mass spectrometry (LC-HRMS). $ONOO^-$ removes the triflate unit by affinity substitution reaction and restored HNTC-HT to fluorophore HNTC-OH. As a conjugated bridge, naphthalene is more suitable for constructing fluorophore with longer wavelength emission. Its photophysical properties are regulated by the type of π-bridge and the relative positions of D and A, and the naphthalene bridging fluorophore has a longer emission wavelength than the previous benzene bridging fluorophore [36]. The fluorescence redshift of HNTC-OH, experimental measurements and theoretical calculations have all confirmed its strong ICT) process. HNTC-HT is the first $ONOO^-$-responsive probe applied to the in vivo differentiation of Hashimoto's thyroiditis against thyroid cancer. It exhibits the long emission wavelength at 737 nm, and also has photostability, selectivity, cytotoxicity and biosafety. It can quantitatively detect $ONOO^-$ in the range of 0–45 μM. The detection limit can be calculated as low as 0.29 μM by limit of detection (LOD) = 3σ/k. In cell experiments, HNTC-HT showed the advantage of effectively distinguishing inflammatory thyroid cells from various types of cancerous thyroid cells. In addition, we established mouse models of thyroid cancer and Hashimoto's thyroiditis. By injecting HNTC-HT into mice models, mice with Hashimoto's thyroiditis were successfully lit up, while the mice with thyroid cancer were not lit up. Thus, the potential of HNTC-HT was confirmed for sensitive discrimination Hashimoto's thyroiditis from thyroid cancer, and the diagnosis accuracy was increased.

2. Experimental section

2.1. Materials and instruments

All relevant reagents and instruments have been described in the Supporting Information. Fluorophore HNTC-OH was synthesized and

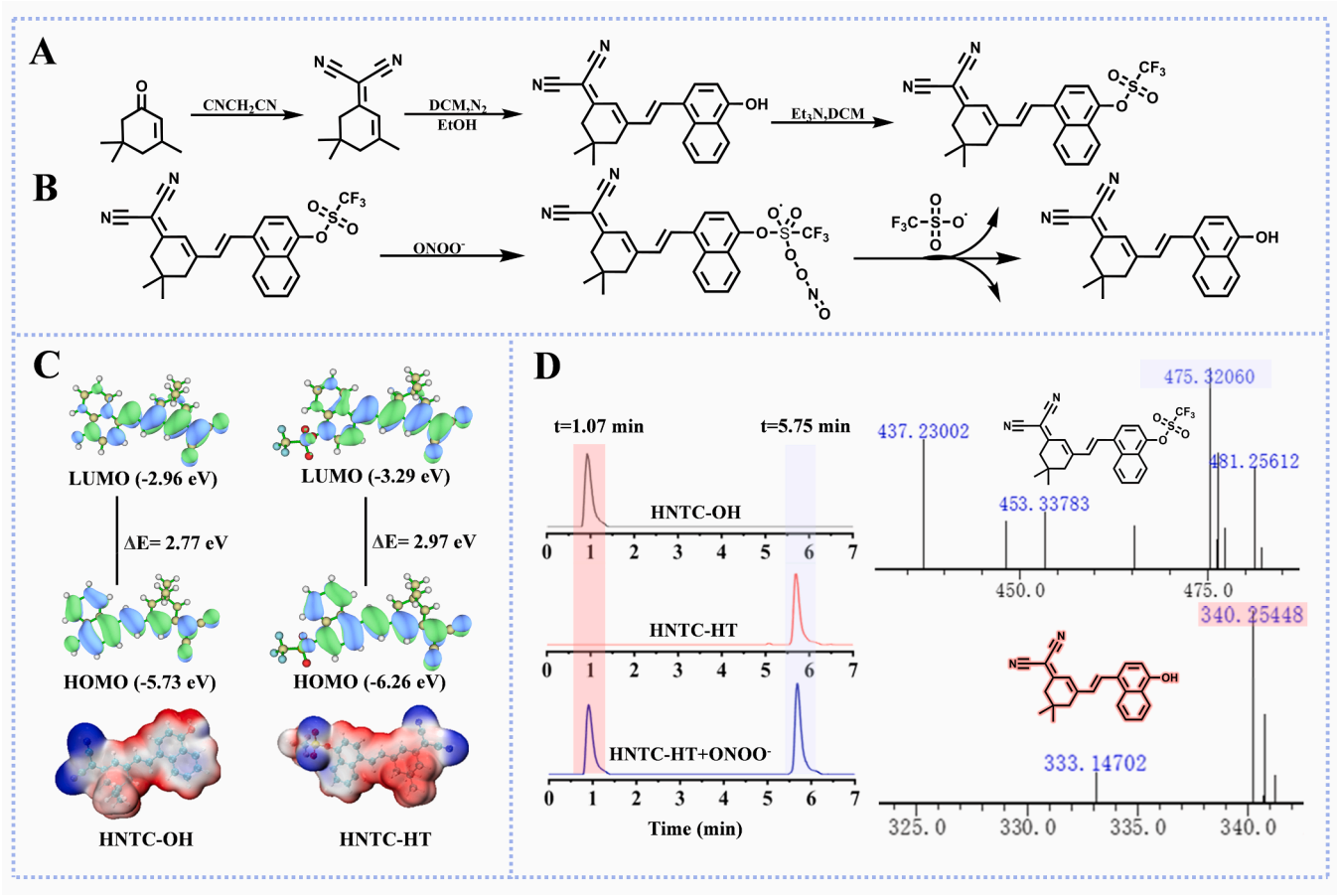

Fig. 1. (A) Synthesis process of HNTC-HT. (B) Proposed response mechanism toward $ONOO^-$ of HNTC-HT. (C) DFT-calculation results for HNTC-OH and HNTC-HT. (D) Response mechanism of HNTC-HT to $ONOO^-$ verified by LC-MS.

characterized by existing methods and the specific structural descriptions are also shown in Supporting Information.

2.2. Synthesis of HNTC-HT

Figs. S1-S4 show the necessary spectra of compound 1 and HNTC-OH (including ^1H NMR and MS spectra). The synthesis of HNTC-HT is shown in Fig. 1A. In N_2 atmosphere, HNTC-OH (290 mg, 1 mmol) was dissolved in 10 mL of mixed solvent (pyridine/CH_2Cl_2, 1:1), cooled in an ice bath for 10 min, then slowly added trifluoromethanesulfonic anhydride (282 mg, 1 mmol) and stirred at room temperature for 30 min. The yellow product was purified by silica gel column chromatography using CH_2Cl_2/MeOH (v/v, 100:1) as eluent. ^1H NMR (300 MHz, $CDCl_3$): δ 8.16 (tq, J = 7.7, 2.3 Hz, 2 H), 7.82 – 7.65 (m, 4 H), 7.51 (d, J = 8.2 Hz, 1 H), 7.07 (d, J = 15.9 Hz, 1 H), 6.93 (s, 1 H), 2.63 (d, J = 18.1 Hz, 4 H), 1.14 (s, 6 H). ^{13}C NMR (75 MHz, $CDCl_3$) δ 168.92, 152.77, 146.16, 133.90, 133.47, 132.43, 131.67, 128.08, 126.59, 124.73, 124.69, 123.89, 123.65, 121.63, 117.70, 113.15, 112.39, 42.98, 39.36, 32.08, 28.05. HR-MS (m/z): Calculated for $[C_{24}H_{20}F_3N_2O_3S]^+$: 475.3206, found: 475.3206 (Figs. S5–S7).

2.3. Spectrophotometric measurement

HNTC-HT was dissolved using dimethyl sulfoxide (DMSO) to obtain an initial solution (1.0 mM). Then in the spectral experiment, HNTC-HT (5.0 μM) was stored in phosphate buffered saline (PBS) buffer, and added $ONOO^-$ at 37 ℃ for 40 min.

2.4. Cell culture and fluorescence imaging

Nthy-ori3–1, 8305 C, FTC, TT cells were incubated in DMEM containing 10 % FBS. The cells were cultured in an incubator with a constant temperature humidifier at 37 ℃, 5 % CO_2/95 % air. The nutrient medium was removed, and the cells were washed three times for further imaging. Fluorescence images of the above cells were acquired with fluorescence inversion microscopy. Additional materials and methods were described in the Supporting Information.

2.5. Fluorescence imaging in thyroid cancer and Hashimoto's disease models of mice

The animal experiment was carried out under the ethical protocols set by Jilin University's Institutional Animal Care and Use Committee (IACUC), certified by ethical inspection permit number SY202409008. Hashimoto's thyroiditis mice models were established as following: First, water-in-oil emulsion was prepared by homogenizing porcine thyroglobulin (PTg) with complete Freund's adjuvant (CFA) at 1:1 (v/v) ratio to achieve final PTg concentration of 0.25 mg/mL. The resulting emulsion was administered at multiple injection points underneath the dorsal skin of the nude mice at a total dose of 50 μg/animal. The injections were performed once per week over a two-week period. Beginning at the third week, the water-in oil emulsion was replaced by mixing porcine thyroglobulin (PTg) with incomplete Freund's adjuvant (v/v, 1:1) to a final concentration of 0.25 mg/mL and dosage for 3 weeks. The resulting emulsion was administered at multiple injection points at a total dose of 50 μg/animal, as well. The injection sites included the subcutaneous dorsal, neck and abdominal cavity regions.

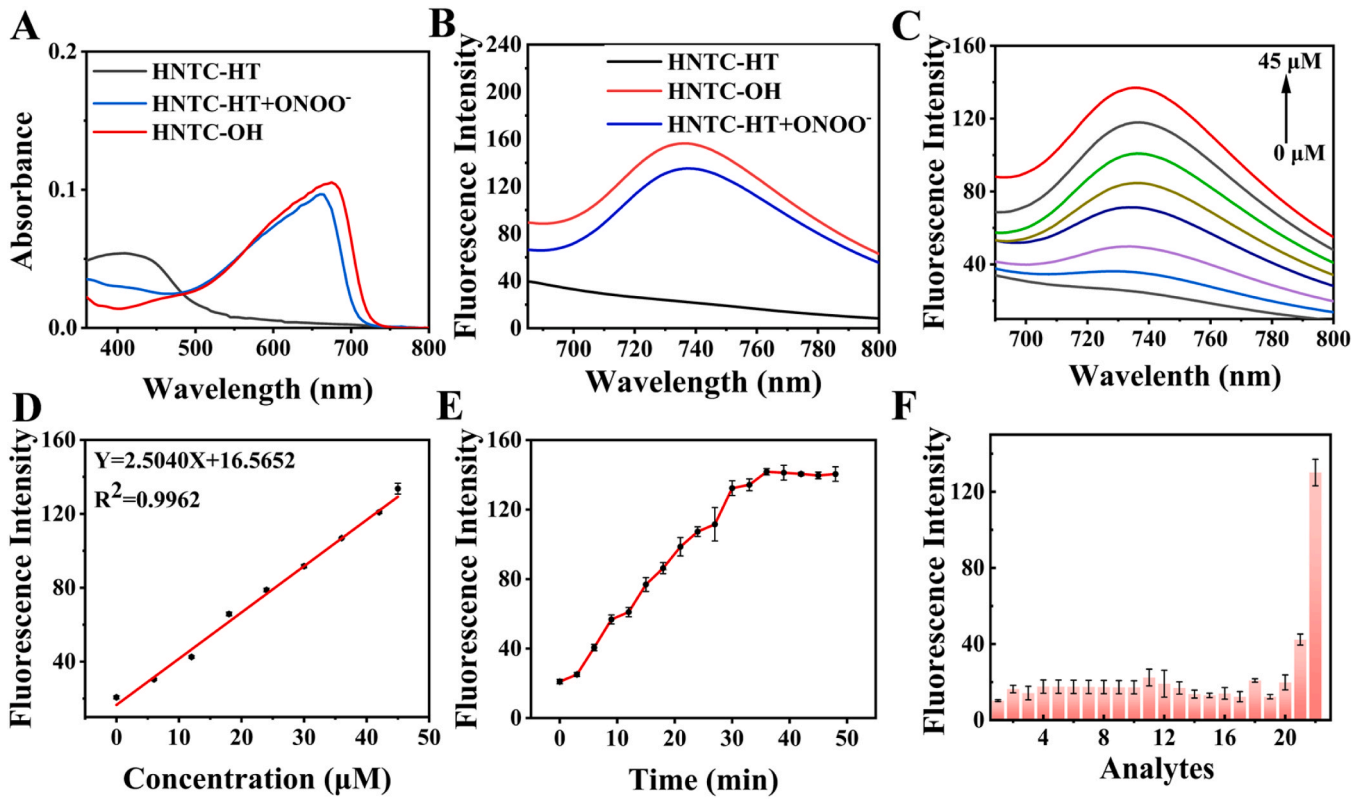

Fig. 2. (A) Absorption spectra of HNTC-HT (1 mM) before and after reaction with 1 mM $ONOO^-$. (B) Fluorescence spectra of HNTC-HT before and after reaction with $ONOO^-$. (C) Spectral profiles of probe HNTC-HT (5 μM) with $ONOO^-$ (0–45 μM). (D) Linear correlation of HNTC-HT (5 μM) and $ONOO^-$ ((0–45 μM). (E) Process of time for detecting $ONOO^-$ (40 μM). (F) Fluorescence intensity of HNTC-HT (5 μM) to different species. (Number :1–22: probe only, Fe^{2+}, K^+, Na^+, Cu^{2+}, Mn^{2+}, Ca^{2+}, Zn^{2+}, Pb^{2+}, Asp, Met, β-Glu, CES1, CES2, Alp, Cys, AChE, BChE, ClO^-, H_2O_2, O_2^-, $ONOO^-$). Solvent system: phosphate PBS/DMSO (1/1, v/v, pH=7.4). λ_{ex} = 665 nm, λ_{em}.= 737 nm

Concurrently, nude mice were provided with high iodine content (0.63 mg/mL). And histological sections of mouse thyroiditis have been made to demonstrate the successful establishment of the inflammation (Fig. S8). Meanwhile, the cancer cells (8305 C) suspension was subcutaneously injected into the thyroid gland of mice, and the tumors were allowed to grow for approximately 3 weeks. At first, nude mice were anesthetized with isoflurane gas and then injected with HNTC-HT (20 μM, 50 μL) subcutaneously on the right side of the nude mice. Imaging is performed separately at specified time intervals to obtain fluorescence responses. Then the mice were randomly divided into control group, Hashimoto's disease (HT) group and thyroid cancer group. HNTC-HT was injected into the above three groups of mice, and the fluorescence imaging results of the three groups were recorded at the imaging time.

3. Results and discussion

3.1. Design, synthesis and reaction mechanism of HNTC-HT

The detailed synthesis route of HNTC-HT is shown in Fig. 1A. HNTC-OH fluorophore is donor-π-acceptor (D-π-A) type fluorophore with hydroxyl group as D, naphthalene as π bridge and dicyano-isoflurone as A. Naphthalene, as a conjugated bridge, is more suitable for constructing fluorophore with longer-wavelength emission, so it is selected as the fluorophore to prepare the probe HNTC-HT. HNTC-OH exhibited a strong ICT process due to the typical D-π-A structure [37,38]. As a strong electron-withdrawing group, the trifluoromethanesulfonic acid group can effectively interrupt the ICT process of HNTC-OH, resulting in fluorescence quenching (Fig. 1C). HNTC-HT reacts nucleophilic ally with $ONOO^-$, and the triflate unit is replaced. Thus, fluorescence effectively recovered (Fig. 1B). Meanwhile, the response mechanism between HNTC-HT and $ONOO^-$ was further proved by LC-MS (Fig. 1D).

3.2. Spectral response

In PBS/DMSO solution, the UV absorption spectra of HNTC-HT before and after reaction with $ONOO^-$ were studied. As shown in Fig. 2A, when $ONOO^-$ (45 μM) was added, the absorption spectra of HNTC-HT at 381 nm is significantly redshifted to 665 nm. And the fluorescence emission spectrum at 737 nm is significantly increased, which indicates that HNTC-HT effectively response to $ONOO^-$ (Fig. 2B). Then, we investigated the ability of HNTC-HT for detecting $ONOO^-$. In the fluorescence titration experiment, after gradually adding $ONOO^-$ (0–50 μM), the new fluorescence peak at 737 nm significantly enhanced (Fig. 2C). Meanwhile, the fluorescence signal intensity at 737 nm showed a good linear relationship with $ONOO^-$ in the concentration range of 1–45 μM, and the linear equation is $y = 2.5040x + 16.5652$, $R^2 = 0.9962$, $r = 0.9981$ (Fig. 2D). We further test the time-dependent emission response of HNTC-HT to $ONOO^-$. As illustrated in Fig. 2E, the fluorescence intensity of HNTC-HT enhanced rapidly, and the reaction reached a plateau within 30 min, indicating that the probe HNTC-HT can response to $ONOO^-$ efficiently and quickly. Meanwhile, the selectivity of the HNTC-HT on different interfering substances was further investigated. The interfering substances include ion, common amino acid, enzyme and reactive oxygen such as Fe^{2+}, K^+, Na^+, Cu^{2+}, Mn^{2+}, Ca^{2+}, Zn^{2+}, Pb^{2+}, Asp, Met, β-Glu, CES1, CES2, Alp, Cys, AChE, BChE, ClO^-, H_2O_2 and O_2^-. After incubation of HNTC-HT with them for 30 min, the fluorescence signal was very weak compared to $ONOO^-$ (Fig. 2F). Therefore, HNTC-HT can selectively detect $ONOO^-$ in dynamic and complex organisms.

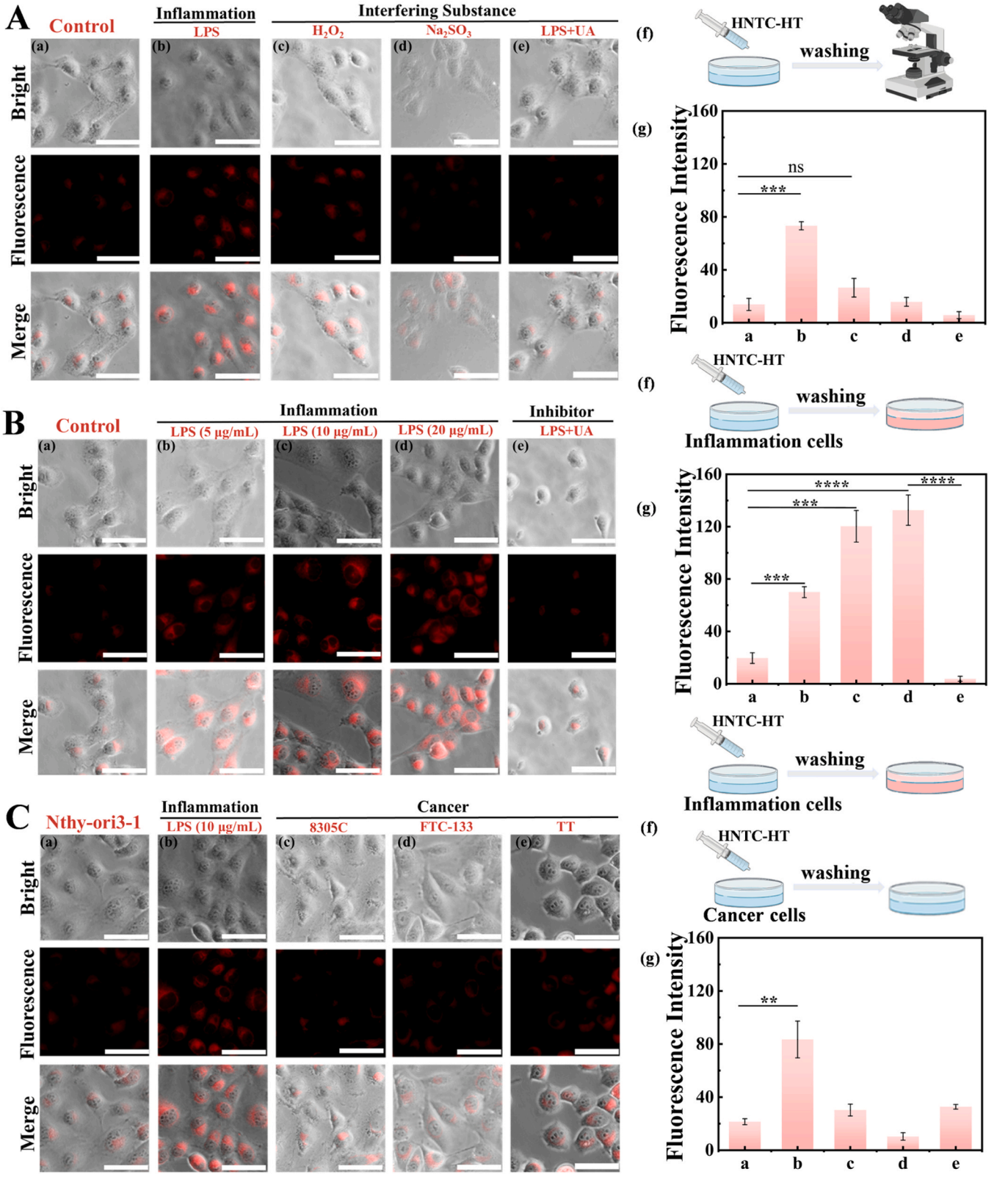

Fig. 3. In vitro fluorescence imaging in living cells with different treatments before incubation. (A) (a) Intact cells; (b) Cells pretreated with LPS (10 μg/mL) for 12 h; (c) Cells pretreated with H_2O_2 (100 μM) for 30 min; (d) Cells pretreated with SO_3^{2-} (100 μM) for 30 min; (e) Cells pretreated with LPS (10 μg/mL) and UA (300 μM) for 12 h. (B) (a) Intact cells; (b) Cells were treated with HNTC-HT (10 μM) alone for 0.5 h; (c) Cells were pre-treated with LPS (5 μg/mL) for 10 h, then cocultured with HNTC-HT (10 μM) for 0.5 h; (d) Cells were pre-treated with LPS (20 μg/mL) for 10 h, then cocultured with 10 μM HNTC-HT for 0.5 h; (e) Cells were pretreated with LPS (5 μg/mL) further cocultured with uric acid (UA, 200 μM) for 0.5 h, followed by HNTC-HT (10 μM) staining for 0.5 h. (C) (a) Nthy-ori3–1 cells following 0.5 h incubation with 10 μM HNTC-HT; (b) Nthy-ori3–1 cells after 12 h incubation with 10 μg/mL LPS, subsequently treated with 10 μM HNTC-HT for 0.5 h; (c) 8305 C cells after a 0.5 h incubation with 10 μM HNTC-HT; (d) FTC-133 cells after 0.5 h incubation with 10 μM HNTC-HT; (e) TT cells after 0.5 h incubation with 10 μM HNTC-HT. λ_{ex} = 605–640 nm, λ_{em} = 715–800 nm. Scale bar: 200 μm.

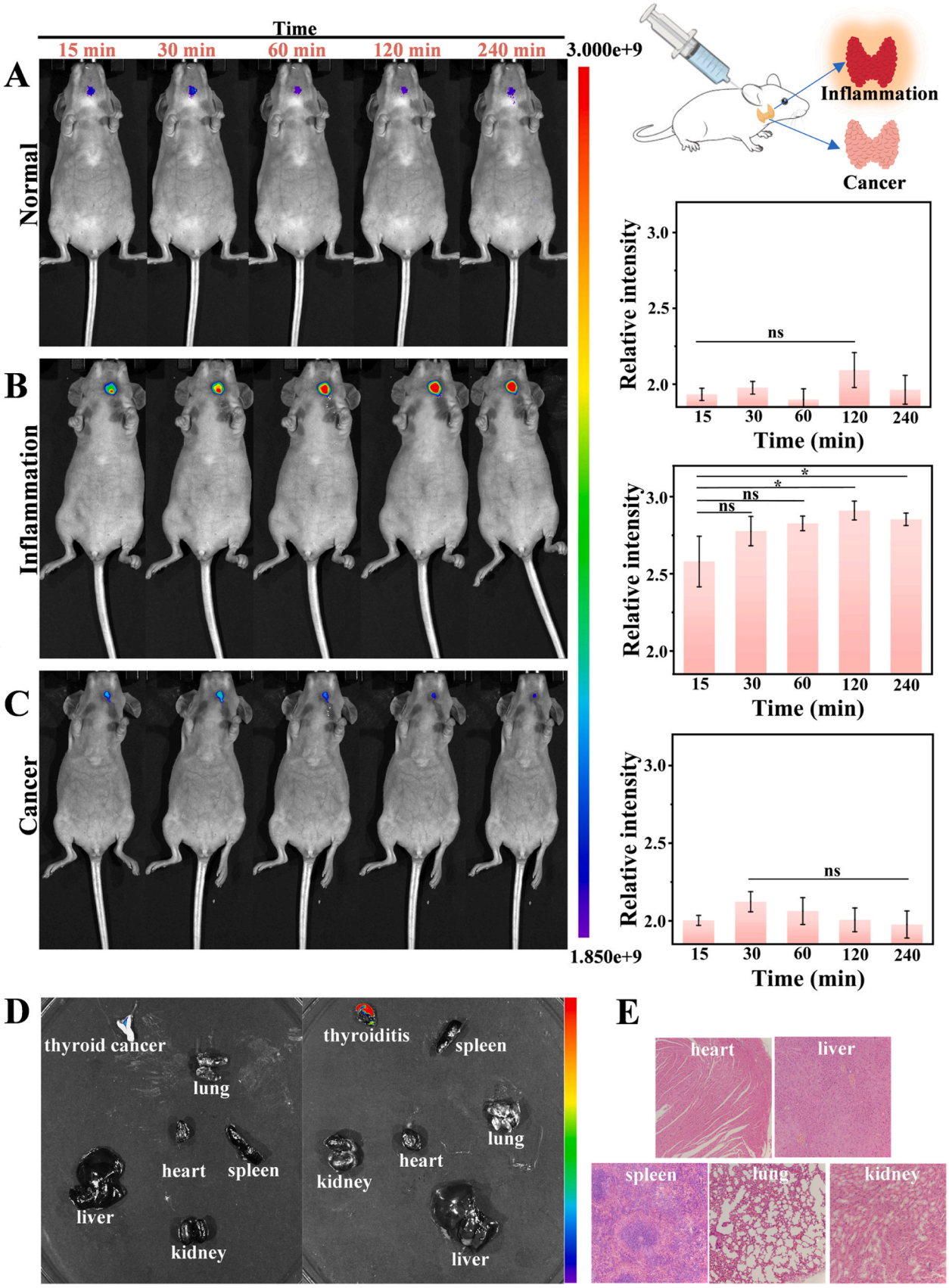

Fig. 4. (A) Normal mice; (B) Hashimoto's thyroiditis mice; (C) Mice with thyroid cancer. (D) Images of major internal organs, thyroiditis tissue and thyroid tumor. (E) H&E staining of pathological sections of different organs in mice (×20 magnification).

We also evaluated the light stability of HNTC-HT before and after its response to $ONOO^-$. Under continuous excitation, the fluorescence intensity of the solution was almost unaffected, indicating that HNTC-HT has excellent photostability (Fig. S9). At the same time, we also verify that the response ability of the probe is not affected in the temperature range of 23–42 ℃ (Fig. S10). In addition, we further investigated the imaging capabilities of HNTC-HT in different pH buffer solutions (Fig. S11). In the absence of $ONOO^-$, it exhibits low fluorescence intensity in the pH range of 6–9. While after the addition of $ONOO^-$, the HNTC-HT exhibited strong fluorescence at 737 nm in the pH range of 6–9. The experimental phenomenon shows that HNTC-HT is effective under physiological pH conditions. All these Above results indicate that HNTC-HT has the ability to specifically detect $ONOO^-$ under complex physiological conditions and great practical application value in complex cellular environments and even in living organisms.

3.3. Imaging of $ONOO^-$ in living cells

Based on above assay results of complex physiological conditions, we continue to explore the feasibility of detecting $ONOO^-$ in living cells. First, we performed hemolysis test assay and Cell Counting Kit-8 (CCK-8) to investigate the cytotoxicity of the HNTC-HT. HNTC-HT exhibited excellent biocompatibility (Fig. S12). As shown in Fig. S13, the cell survival rate remained above 80 % even at high concentrations of the HNTC-HT. These results indicated the biosecurity of probe. Then we investigated the ability of HNTC-HT to image endogenous $ONOO^-$ in living cells. Following 30 min co-incubation with the probe, cells exhibited stabilized fluorescence intensity (Fig. S14). As shown in Fig. 3A, Nthy-ori3–1 cells (a cell line derived from normal human thyroid tissue) treated with HNTC-HT showed a weak fluorescence signal, indicating that the content of $ONOO^-$ was relatively low under normal conditions, then the fluorescence intensity increased significantly after incubation with lipopolysaccharide (LPS) to induce inflammatory response for 12 h. At the same time, in order to eliminate the potential interference caused by other biological oxidants and nucleophiles in the organism, further selective determination was performed in the cells·H_2O_2 and SO_3^{2-} are selected as oxidant and nucleophile to further evaluate its anti-interference. When the cells were pretreated with H_2O_2 or SO_3^{2-}, only weak fluorescence was observed, in contrast to the significant fluorescence enhancement observed when the cells were treated with LPS. Meanwhile, in the presence of UA ($ONOO^-$ inhibitor), intracellular fluorescence was significantly lowered. The intracellular selectivity experiments proved that HNTC-HT was only responsive to $ONOO^-$ specifically in living cells. In addition, the fluorescence intensity of the cells gradually increased with the increase of the concentration of LPS used to pretreat the cells in Fig. 3B. These results indicated that HNTC-HT can image $ONOO^-$ in living cells accurately.

Next, we compared fluorescence intensity of the cells induced by endogenous inflammation with three thyroid cancer subtypes: undifferentiated carcinoma of thyroid gland (8305 C), follictalar thyroid carcinoma (FTC) and medullary thyroid carcinoma (TT). As shown in Fig. 3C, the fluorescence intensity of inflammatory thyroid cells was significantly stronger than that of normal thyroid cells Nthy-ori3–1, and also stronger than that of three other thyroid cancer subtypes. This finding implied that HNTC-HT could effectively differentiate inflammatory thyroid cells from carious major thyroid cancer cells. Thus, it has great potential applications in differentiating thyroiditis tissue against thyroid cancer tissue.

3.4. Imaging of normal mice, HT mice, and thyroid cancer mice in vivo

In order to further verify the ability in differ entail diagnosis of thyroid diseases with HNTC-HT, we established mice models of Hashimoto's thyroiditis and thyroid cancer. As shown in Fig. 4A, B and C, the thyroid site of the Hashimoto's thyroiditis mice showed a significantly stronger fluorescence signal after HNTC-HT injection. In contrast, mice with thyroid cancer and normal mice showed only weak fluorescence signals. This is consistent with the results from the cell experiments described above. After the extended time period, a slight increase in the fluorescence signal was observed in the same group of mice. Although the fluorescence signals of these three kinds of mice were slightly stronger with the extension of time, the difference of the overall fluorescence signals remained stable, which indicated that HNTC-HT had strong anti-interference ability in mice. Moreover, as shown in Fig. 4D, the fluorescence intensity of thyroid cancer tissue was also significantly weaker than the fluorescence of inflammatory thyroid tissue. Meanwhile, the fluorescence signals of heart, liver, spleen, lung, and kidney could be ignored, indicating that thyroiditis tissue tumor could be distinguished against thyroid cancer through the reaction of high expression of $ONOO^-$ with HNTC-HT in vivo. H&E staining of tissue sections (Fig. 4E) showed that no significant organ damage in major organs of mice after injecting HNTC-HT, which confirmed the biosafety of the probe. And the control experiments with DMSO/PBS injections in normal mice confirmed the absence of background fluorescence, systematically eliminating solvent interference in our imaging results (Fig. S15).

4. Conclusion

In summary, we have constructed a NIR-fluorescent probe HNTC-HT with a large Stokes shift, which are used for differentiated imaging of Hashimoto's thyroiditis against thyroid carcinoma by endogenous $ONOO^-$. HNTC-HT was synthesized with dicyano-isoflurone. $ONOO^-$ removes the trifluoromethanesulfonic acid group from the probe by nucleophilic substitution reaction and generates fluorescence signal by restoration of ICT process. In spectroscopic experiments, HNTC-HT can respond to $ONOO^-$ within 5 min, and the fluorescence intensity is finally enhanced 7–8 times. It also has excellent sensitivity and selectivity for $ONOO^-$ detection in various biological oxidants and nucleophilic reagents. Moreover, it could be used to monitor endogenous $ONOO^-$ by inverted fluorescence microscope with excellent performance in cell and tissue imaging. Furthermore, HNTC-HT was first time to visualize the inflammatory thyroid cells related to $ONOO^-$ levels in mice and differentiate Hashimoto's thyroiditis tissue against cancerous tissue sensitively and rapidly. Taken together, the novel probe HNTC-HT exhibits significant ability in differentiating imaging Hashimoto's thyroiditis from thyroid cancer both in vitro and in vivo, thereby enhancing the accuracy of thyroid disease diagnosis.

CRediT authorship contribution statement

Mo Ma: Visualization, Formal analysis. **Wanwei Zhang:** Writing – original draft, Methodology, Formal analysis. **Wenping Dong:** Software, Data curation. **Chen Zhao:** Validation, Investigation. **Daqian Song:** Methodology, Funding acquisition. **Pinyi Ma:** Methodology, Funding acquisition. **Ying Sun:** Writing – review & editing, Project administration, Methodology.

Declaration of Competing Interest

The authors declare that they have no known competing financial interests or personal relationships that could have appeared to influence the work reported in this paper.

Acknowledgments

The National Natural Science Foundation of China (22074052 and 22004046) and the Science and Technology Developing Foundation of Jilin Province of China (20230101033JC).

Appendix A. Supporting information

Supplementary data associated with this article can be found in the online version at doi:10.1016/j.snb.2025.138268.

Data availability

Data will be made available on request.

References

[1] Q.-Y. Zhang, X.-P. Ye, Z. Zhou, C.-F. Zhu, R. Li, Y. Fang, et al., Lymphocyte infiltration and thyrocyte destruction are driven by stromal and immune cell components in Hashimoto's thyroiditis, Nat. Commun. 13 (2022) 775.
[2] R. Li, T. He, Z. Xing, L. Mi, A. Su, W. Wu, The immune system in Hashimoto's thyroiditis: updating the current state of knowledge on potential therapies and animal model construction, Autoimmun. Rev. 24 (2025) 103783.
[3] M. Ralli, D. Angeletti, M. Fiore, V. D'Aguanno, A. Lambiase, M. Artico, et al., Hashimoto's thyroiditis: an update on pathogenic mechanisms, diagnostic protocols, therapeutic strategies, and potential malignant transformation, Autoimmun. Rev. 19 (2020) 102649.
[4] K. Kakudo, Y. Bai, S. Katayama, M. Hirokawa, Y. Ito, A. Miyauchi, et al., Classification of follicular cell tumors of the thyroid gland: analysis involving Japanese patients from one institute, Pathol. Int. 59 (2009) 359–367.
[5] X.-h Liu, H.-q Yin, H. Shen, X.-Y. Wang, Z. Zhang, X.-f Yuan, et al., A multivariable model of ultrasound and biochemical parameters for predicting high-volume lymph node metastases of papillary thyroid carcinoma with Hashimoto's thyroiditis, Front. Endocrinol. 15 (2025) 1501142.
[6] L. Zhang, H. Li, Q.-h Ji, Y.-x Zhu, Z.-y Wang, Y. Wang, et al., The clinical features of papillary thyroid cancer in Hashimoto's thyroiditis patients from an area with a high prevalence of Hashimoto's disease, BMC Cancer 12 (2012) 610.
[7] L.B. Woolner, W.M. McConahey, O.H. Beahrs, Struma lymphomatosa (Hashimoto's thyroiditis) and related thyroidal disorders, J. Clin. Endocrinol. Metab. 19 (1959) 53–83.
[8] D. Ahn, S.J. Heo, J.H. Park, J.H. Kim, J.H. Sohn, J.Y. Park, et al., Clinical relationship between Hashimoto's thyroiditis and papillary thyroid cancer, Acta Oncol. 50 (2011) 1228–1234.
[9] E. Farrell, C. Heffron, M. Murphy, G. O'Leary, P. Sheahan, Impact of lymphocytic thyroiditis on incidence of pathological incidental thyroid carcinoma, Head. Neck 39 (2016) 122–127.
[10] B. Jankovic, K.T. Le, J.M. Hershman, Hashimoto's thyroiditis and papillary thyroid carcinoma: is there a correlation? J. Clin. Endocrinol. Metab. 98 (2013) 474–482.
[11] C. Giordano, G. Stassi, R. De Maria, M. Todaro, P. Richiusa, G. Papoff, et al., Potential involvement of Fas and its ligand in the pathogenesis of Hashimoto's thyroiditis, Science 275 (1997) 960.
[12] R.D. Abbott, A. Sadowski, A.G. Alt, Efficacy of the autoimmune protocol diet as part of a multi-disciplinary, supported lifestyle intervention for Hashimoto's thyroiditis, Cureus 11 (2019) 4556.
[13] N. Daramjav, J. Takagi, H. Iwayama, K. Uchino, D. Inukai, K. Otake, et al., Autoimmune thyroiditis shifting from Hashimoto's thyroiditis to Graves' disease, Medicina 59 (2023) 757.
[14] M.P. Kumarasinghe, S.D. Silva, Pitfalls in cytological diagnosis of autoimmune thyroiditis, Pathology 31 (1999) 010001–010007.
[15] T. Zheng, C. Xu, C. Mao, X. Mou, F. Wu, X. Wang, et al., Increased interleukin-23 in hashimoto's thyroiditis disease induces autophagy suppression and reactive oxygen species accumulation, Front. Endocrinol. 9 (2018) 00096.
[16] M.L. Gheorghiu, C. Badiu, Selenium involvement in mitochondrial function in thyroid disorders, Hormones 19 (2020) 25–30.
[17] R.M. Ruggeri, T.M. Vicchio, M. Cristani, R. Certo, D. Caccamo, A. Alibrandi, et al., Oxidative stress and advanced glycation end products in Hashimoto's thyroiditis, Thyroid 26 (2016) 504–511.
[18] J.-H. Koh, M.W. Pataky, S. Dasari, K.A. Klaus, I. Vuckovic, G.N. Ruegsegger, et al., Enhancement of anaerobic glycolysis – a role of PGC-1α4 in resistance exercise, Nat. Commun. 13 (2022) 2324.
[19] R.-X. Wang, Y. Ou, Y. Chen, T.-B. Ren, L. Yuan, X.-B. Zhang, Rational design of NIR-II g-quadruplex fluorescent probes for accurate in vivo tumor metastasis imaging, J. Am. Chem. Soc. 146 (2024) 11669–11678.
[20] J.M. Ku, M.J. Kim, Y.-J. Choi, S.Y. Lee, J.-Y. Im, Y.-K. Jo, et al., JI017 induces cell autophagy and apoptosis via elevated levels of reactive oxygen species in human lung cancer cells, Int. J. Mol. Sci. 24 (2023) 7528.
[21] C. Pan, G. Gu, Novel design of protein-functionalized gold nanoparticles loaded with dichlororuthenium (II) (p-cymene) (1,3,5-triaza-7-phosphaadamantane) (rapta-c) to induce reactive oxygen species (ROS)-mediated apoptosis in ovarian cancer cells, J. Macromol. Sci. Part B Phys. 23 (2024) 74651.
[22] W. Yang, R. Liu, X. Yin, Y. Jin, L. Wang, M. Dong, et al., Peroxynitrite activated near-infrared fluorescent probe for evaluating ferroptosis-mediated acute kidney injury, Sens. Actuators B Chem. 393 (2023) 134180.
[23] Z. Wang, M. Yan, M. Yu, G. Zhang, W. Fang, F. Yu, A fluorescent probe with zwitterionic ESIPT feature for ratiometric monitoring of peroxynitrite in vitro and in vivo, Anal. Chem. 96 (2024) 3600–3608.
[24] M. Yan, M. Yu, Z. Wang, F. Yu, W. Fang, An α-ketoamide-based fluorescent probe via aggregation induced emission for ONOO− detection in vivo, Talanta 293 (2025) 128064.
[25] F. Bedioui, D. Quinton, S. Griveau, T. Nyokong, Designing molecular materials and strategies for the electrochemical detection of nitric oxide, superoxide and peroxynitrite in biological systems, Phys. Chem. Chem. Phys. 12 (2010) 9976–9988.
[26] M. Noel Alvarez, G. Peluffo, L. Piacenza, R. Radi, Intraphagosomal peroxynitrite as a macrophage-derived cytotoxin against internalized, J. Biol. Chem. 286 (2011) 6627–6640.
[27] P. Huang, Z. Li, L. Nong, J. Cheng, W. Lin, A therapeutic probe for detecting and inhibiting ONOO− in senescent cells, Cells J. Mater. Chem. B 11 (2023) 2389–2396.
[28] M.L. Odyniec, S.-J. Park, J.E. Gardiner, E.C. Webb, A.C. Sedgwick, J. Yoon, et al., A fluorescent ESIPT-based benzimidazole platform for the ratiometric two-photon imaging of ONOO− in vitro and ex vivo, Chem. Sci. 11 (2020) 7329–7334.
[29] S. Zhang, M. Ma, J. Li, J. Li, L. Xu, D. Gao, et al., A pyroglutamate aminopeptidase 1 responsive fluorescence imaging probe for real-time rapid differentiation between thyroiditis and thyroid cancer, Anal. Chem. 96 (2024) 5897–5905.
[30] W. Kang, M. Ma, S. Tang, Y. Wang, J. Li, L. Xu, et al., A rapidly metabolizable and enzyme-activated NIR fluorescent probe based on isophorone for imaging in vivo, Sens. Actuators B Chem. 419 (2024) 136299.
[31] L. Dai, Q. Zhang, Q. Ma, W. Lin, Emerging near infrared fluorophore: dicyanoisophorone-based small-molecule fluorescent probes with large stokes shifts for bioimaging, Coord. Chem. Rev. 489 (2023) 215193.
[32] D. Cheng, Y. Pan, L. Wang, Z. Zeng, L. Yuan, X. Zhang, et al., Selective visualization of the endogenous peroxynitrite in an inflamed mouse model by a mitochondria-targetable two-photon ratiometric fluorescent probe, J. Am. Chem. Soc. 139 (2017) 285–292.
[33] F. Yu, P. Li, G. Li, G. Zhao, T. Chu, K. Han, A. NIR, NIR reversible fluorescent probe modulated by selenium for monitoring peroxynitrite and imaging in living cells, J. Am. Chem. Soc. 133 (2011) 11030–11033.
[34] A. Grzelakowska, M. Zielonka, K. Dębowska, J. Modrzejewska, M. Szala, A. Sikora, et al., Two-photon fluorescent probe for cellular peroxynitrite: fluorescence detection, imaging, and identification of peroxynitrite-specific products, Adv, Free Radic. Biol. Med 169 (2021) 24–35.
[35] Z. Huang, L. Shi, H. Liu, Z.K. Zhou, H. Xiang, S. Gong, et al., Rational design of an iminocoumarin-based fluorescence probe for peroxynitrite with high signal-to-noise ratio, Luminescence 39 (2024) 4679.
[36] D. Chen, G. Nie, Y. Dang, W. Liang, W. Li, C. Zhong, Rational design of near-infrared fluorophores with a phenolic D–A type structure and construction of a fluorescent probe for cysteine imaging, N. J. Chem. 45 (2021) 18528–18537.
[37] T. Lu, A comprehensive electron wavefunction analysis toolbox for chemists, Multiwfn, J. Chem. Phys. 161 (2024) 082503.
[38] T. Lu, F. Chen, Multiwfn: a multifunctional wavefunction analyzer, J. Comput. Chem. 33 (2011) 580–592.

Wanwei Zhang is currently a master degree student in College of Chemistry, Jilin University. Her interest is spectral analysis.

Mo Ma is currently a Ph.D. student in School of Pharmacy, Jilin University. His interest is spectral analysis.

Chen Zhao is currently a Ph.D. student in College of Chemistry, Jilin University. Her interest is spectral analysis.

Wenping Dong is currently a master degree student in College of Chemistry, Jilin University. Her interest is spectral analysis.

Pinyi Ma gained his doctor's degree from College of Chemistry, Jilin University in 2017 and he is an associate professor in that school. His research area is spectral analysis.

Daqian Song gained his doctor's degree from College of Chemistry, Jilin University in 2003 and he is a professor in that school. His research areas are spectral and chromatography analysis.

Ying Sun gained her doctor's degree from College of Chemistry, Jilin University in 2009 and she is a professor in that school. Her research area is spectral analysis.